iScience, Volume *23*

Supplemental Information

Systematic Quantification of Synapses in Primary Neuronal Culture

Peter Verstraelen, Gerardo Garcia-Diaz Barriga, Marlies Verschuuren, Bob Asselbergh, Rony Nuydens, Peter H. Larsen, Jean-Pierre Timmermans, and Winnok H. De Vos

Supplemental figures

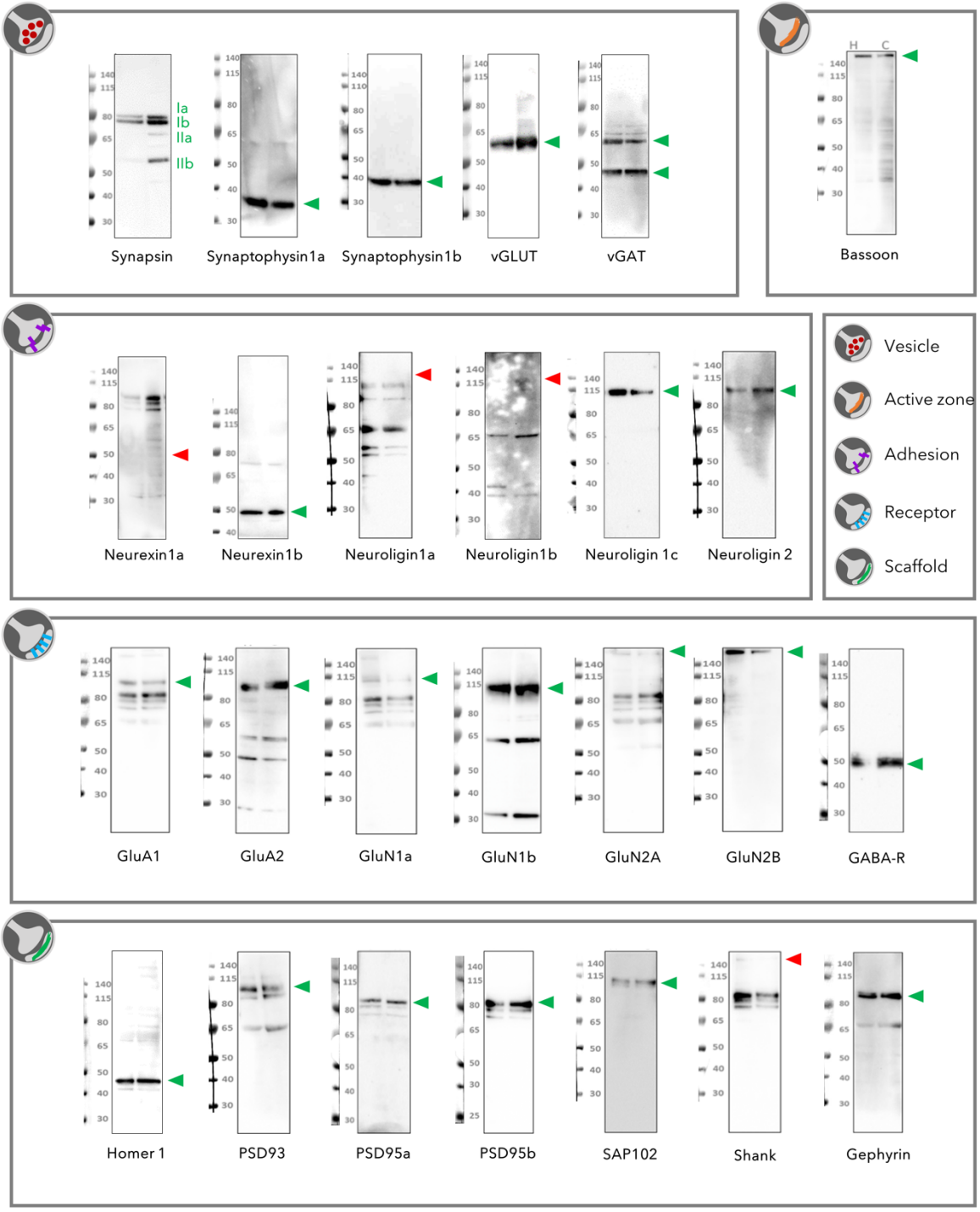

Figure S1. Antibody validation by western blot. (Related to Fig. 1)
Antibodies were tested on lysates of 14 DIV primary hippocampal (left lane) and cortical (right lane) cultures. The molecular weight marker in the visible spectrum is shown on the left. An arrowhead indicates the height of the predicted molecular weight of each marker and is shown in green or red when the predicted band is present or absent, respectively. Additional or missing bands may be the result of alternative isoforms or (un-)masked epitopes due to sample denaturation, which makes the predictive value of immunoblotting for IF performance very weak.

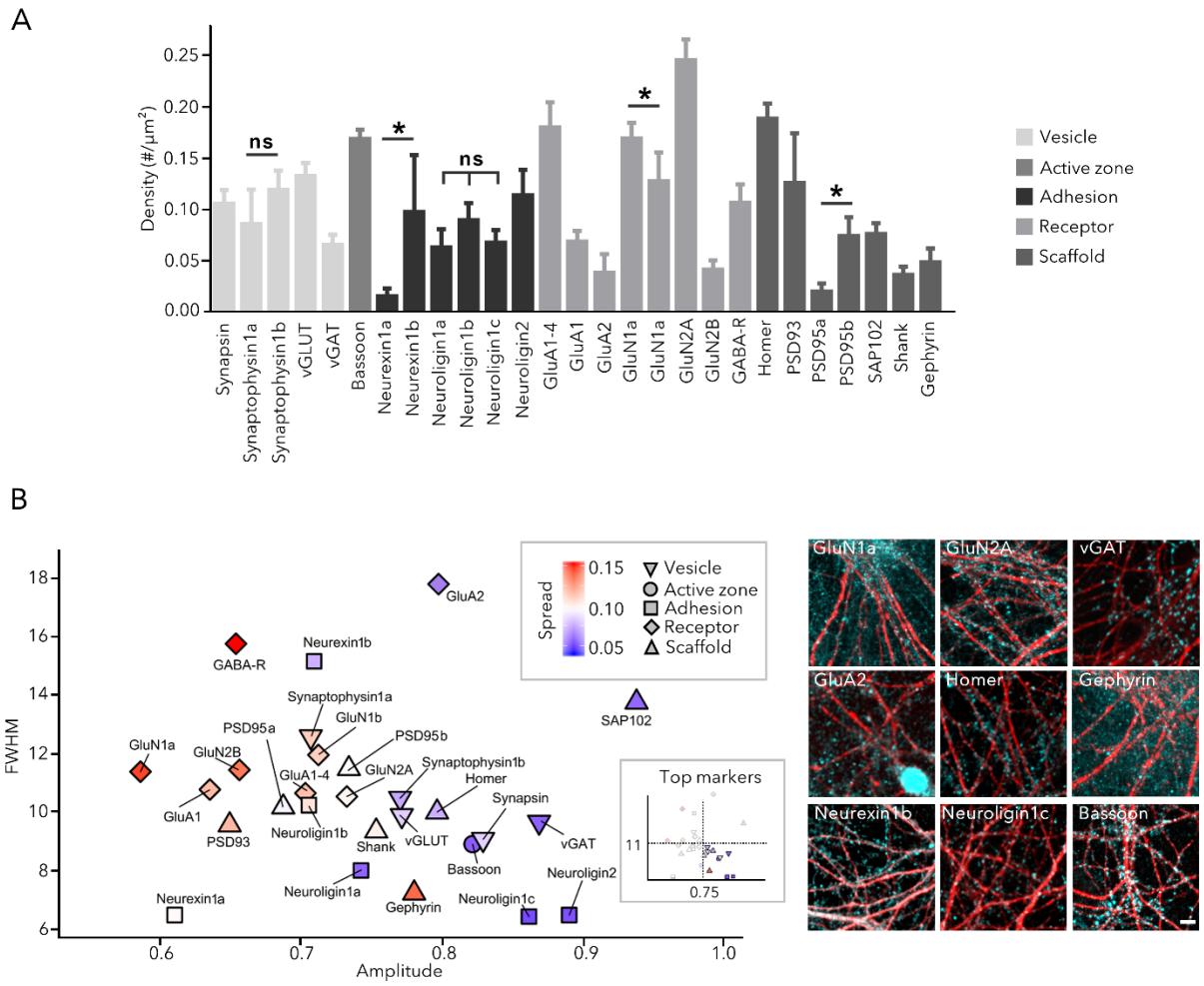

Figure S2. Synapse marker evaluation in 14 DIV primary hippocampal cultures. (Related to Fig. 1)
(A) Quantification of the spot density by manual thresholding reveals variable results (Mean + SD, n=6 wells with 15 fields/well, *p<0.05, one-way ANOVA post-hoc Sidak's multiple comparisons test); (B) Synapse antibody evaluation in 14 DIV primary hippocampal cultures. A scatter plot of ACF-derived parameters (and inset with gating on optimal parameter conditions) along with representative images are shown (n=90 images originating from 6 wells, scale bar 10 µm).

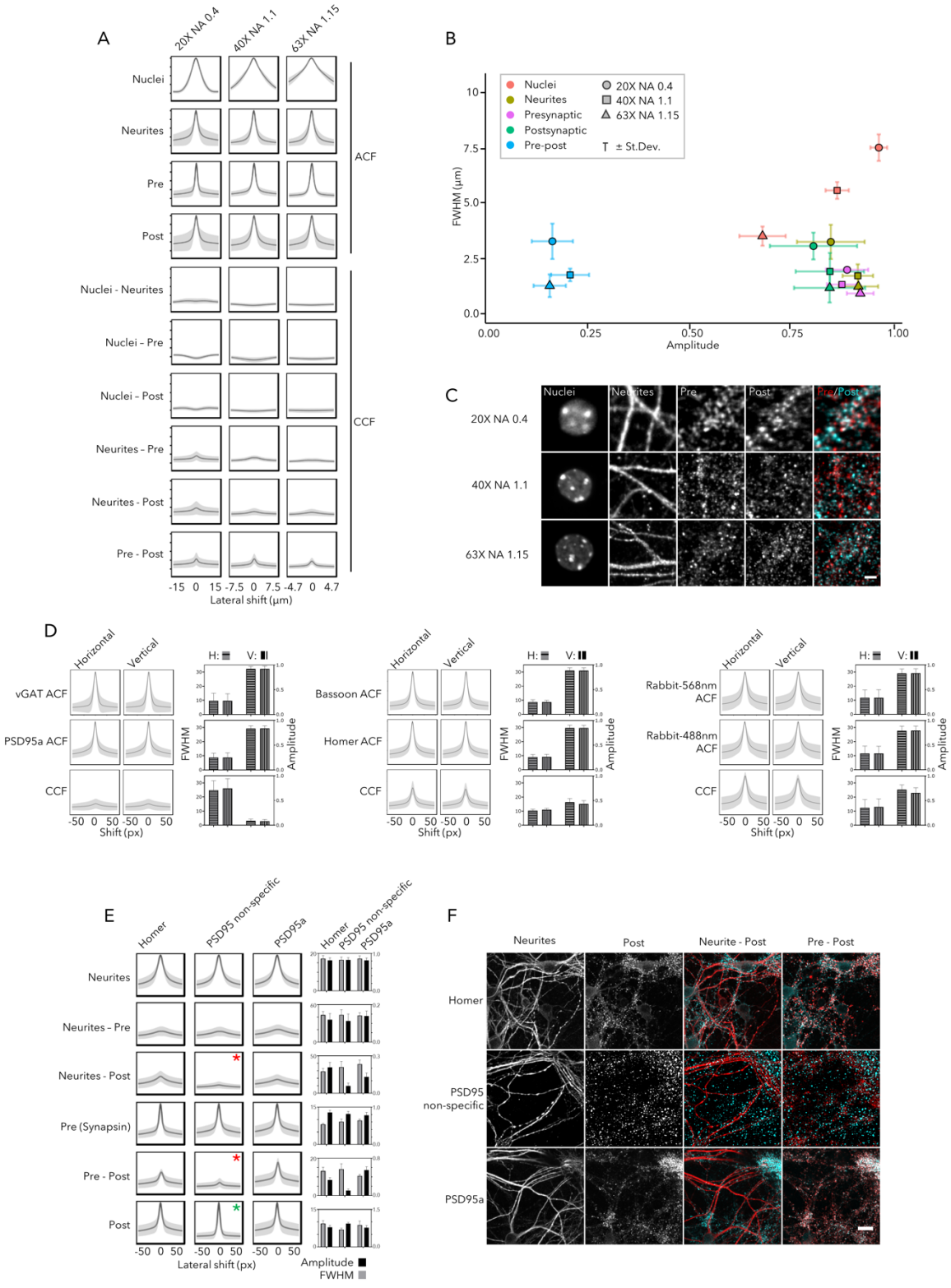

Figure S3. Segmentation-independent analysis of primary neuronal networks. (Related to Fig. 1)
(A-C) ACF/CCF readout depends on the image resolution. (A) ACF and CCF plots for all channel combinations of DAPI (nuclei) / MAP2 (neurites) /Bassoon (Pre) / Homer (Post)-stained primary cortical cultures, acquired with different objective lenses using the same sliding window of 50 pixels. For all markers, the FWHM (in µm) increases

with lower numerical aperture due to the broadening of the point spread function. The more pronounced increase in FWHM for the nuclei channel is most likely due to the chromocenters becoming less resolved and contrasted at lower resolution, causing them to now longer be picked up as individual entities. The amplitude remains largely unchanged, except for the nuclei channel which is due to the sliding window not capturing the whole size of the structure at higher magnifications (n=90 images originating from 6 wells); (B) Scatter plot of the amplitude and FWHM (±std) derived from the ACF/CCF plots shown in panel A; (C) Crops of 30x30 µm from representative images acquired with different objective lenses (scale bar 5 µm); (D) The direction of the lateral shift does not affect the ACF/CCF readout as shown by the non-significant differences in amplitude and FWHM for horizontal vs. vertical ACF / CCF of three marker combinations with different overlap (n=90 images originating from 6 wells); (E) ACF and CCF plots of primary cortical cultures stained for MAP2, Synapsin and one of the above-mentioned postsynaptic markers. In contrast with Homer and PSD95a antibodies, one antibody (PSD95 abcam ab2723) yields non-specific puncta that are uniformly distributed across the image and have a size comparable to that of synaptic spots. This results in a seemingly 'good' ACF readout (green asterisk), yet CCFs indicate that the colocalization with neurites and presynaptic spots is lower than expected (red asterisks), allowing identification of this non-specific antibody (n=90 images originating from 6 wells); (F) Microscopic images confirm the lack of colocalization of the non-specific PSD95 antibody with neurites and the presynaptic marker (scale bar 20 µm).

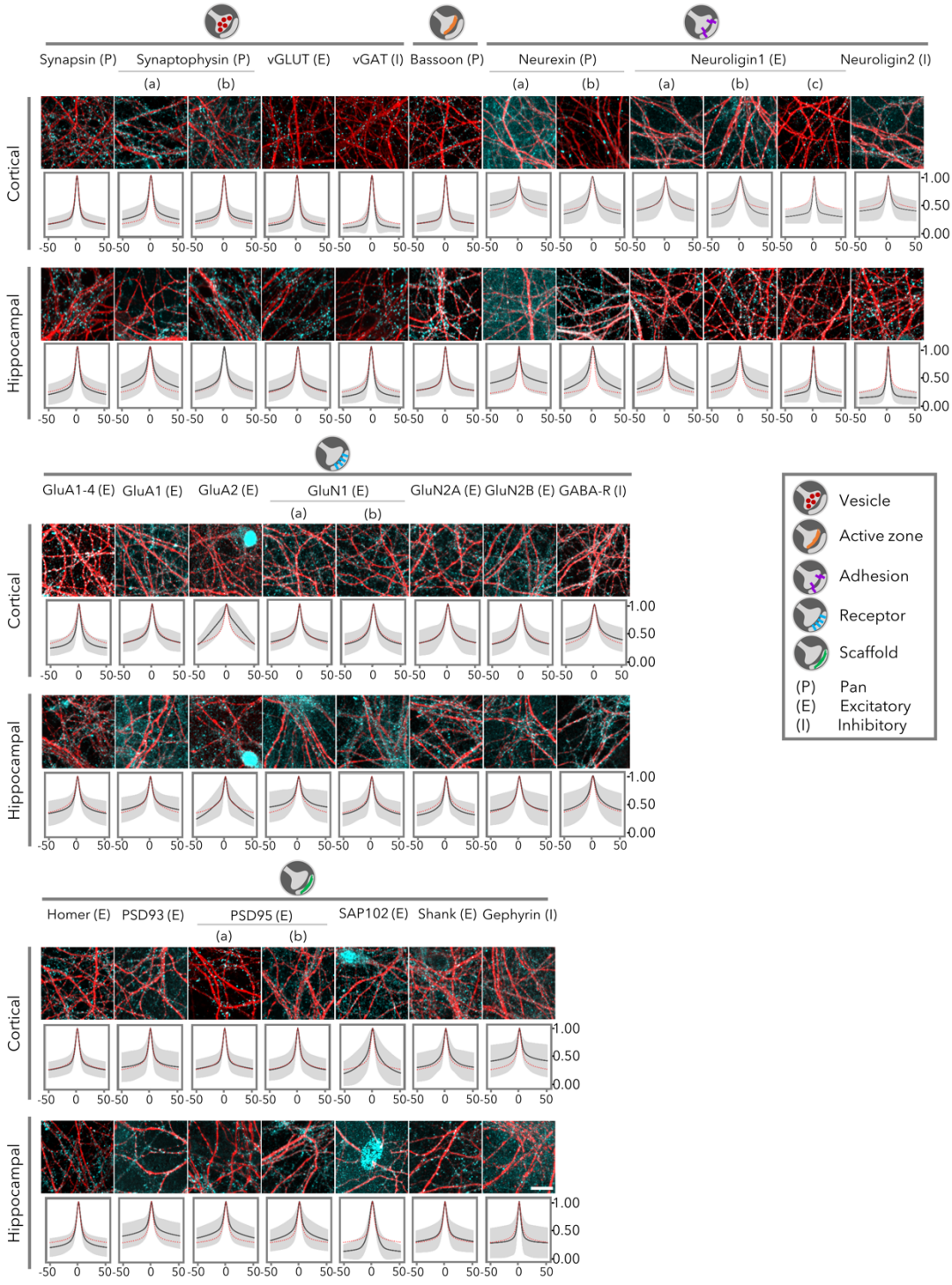

Figure S4. Labeling specificity of synapse marker antibodies. (Related to Fig. 1)
IF results of all tested antibodies on 14 DIV primary cortical and hippocampal cultures are shown, subdivided into five different functional classes (see **Fig. 1a**). A representative image of MAP2 (red) with the synapse marker (cyan - contrast optimized) is shown along with the auto-correlation function (ACF) of the image dataset, which served for extracting amplitude, spread and FWHM in **Fig. 1** (n=90 images originating from 6 wells, scale bar 20 µm). The average ACF of the functional class is superimposed in red.

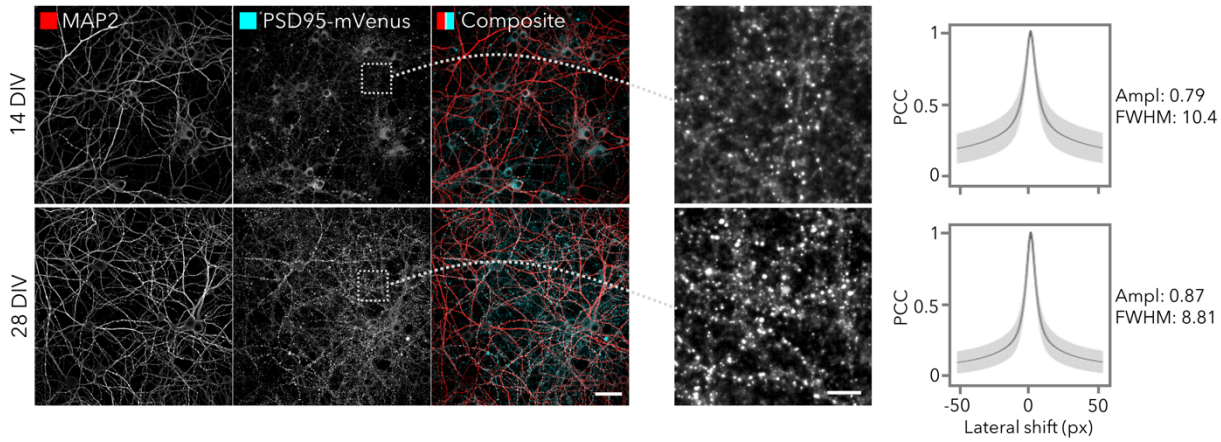

Figure S5. PSD95-mVenus signal evolves between 14 and 28 DIV. (Related to Fig. 2)
Representative images of 14 and 28 DIV cortical cultures. The contrast-matched images reveal a marked increase in the overall intensity of the PSD95-mVenus signal between 14 and 28 DIV (scale bar 50 µm). The insets, shown with optimized contrast settings per DIV, show a larger difference between back- and foreground for 28 as compared to 14 DIV (scale bar 10 µm), leading to an ACF with higher amplitude (n=90 images originating from 6 wells). Note that the ACF relies on the Pearson's Correlation Coefficient (PCC) which is independent of the average intensity.

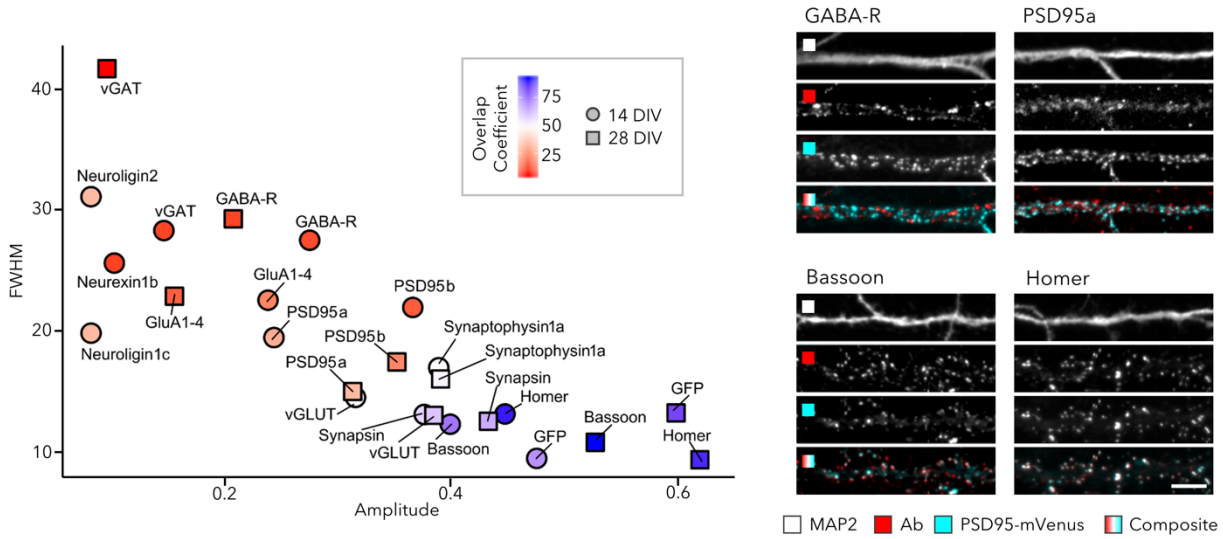

Figure S6. Colocalization of synapse marker antibodies with PSD95-mVenus in primary hippocampal cultures. (Related to Fig. 2)
The colocalization is shown as a scatter plot of the CCF-derived parameters amplitude (reporting on colocalization) and FWHM (reporting on combined size), and colored by the overlap coefficient (OC), defined as the percentage of PSD95-mVenus spots that have an overlapping antibody spot (n=90 images originating from 6 wells). Images are from 28 DIV hippocampal cultures (scale bar 10 µm).

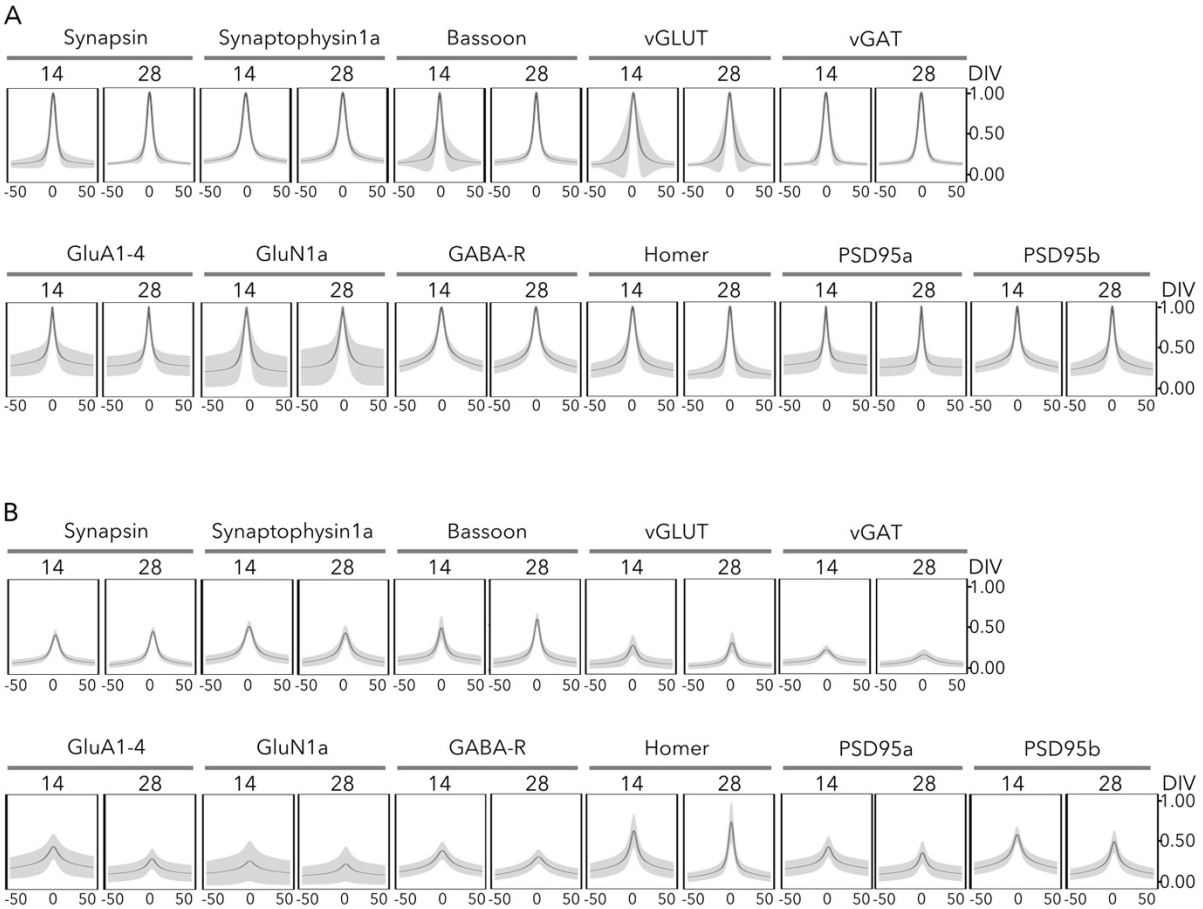

Figure S7. Auto- (A) and cross-correlation (B) functions of PSD95-mVenus and synapse markers in cortical cultures (n=90 images originating from 6 wells). (Related to Fig. 2)

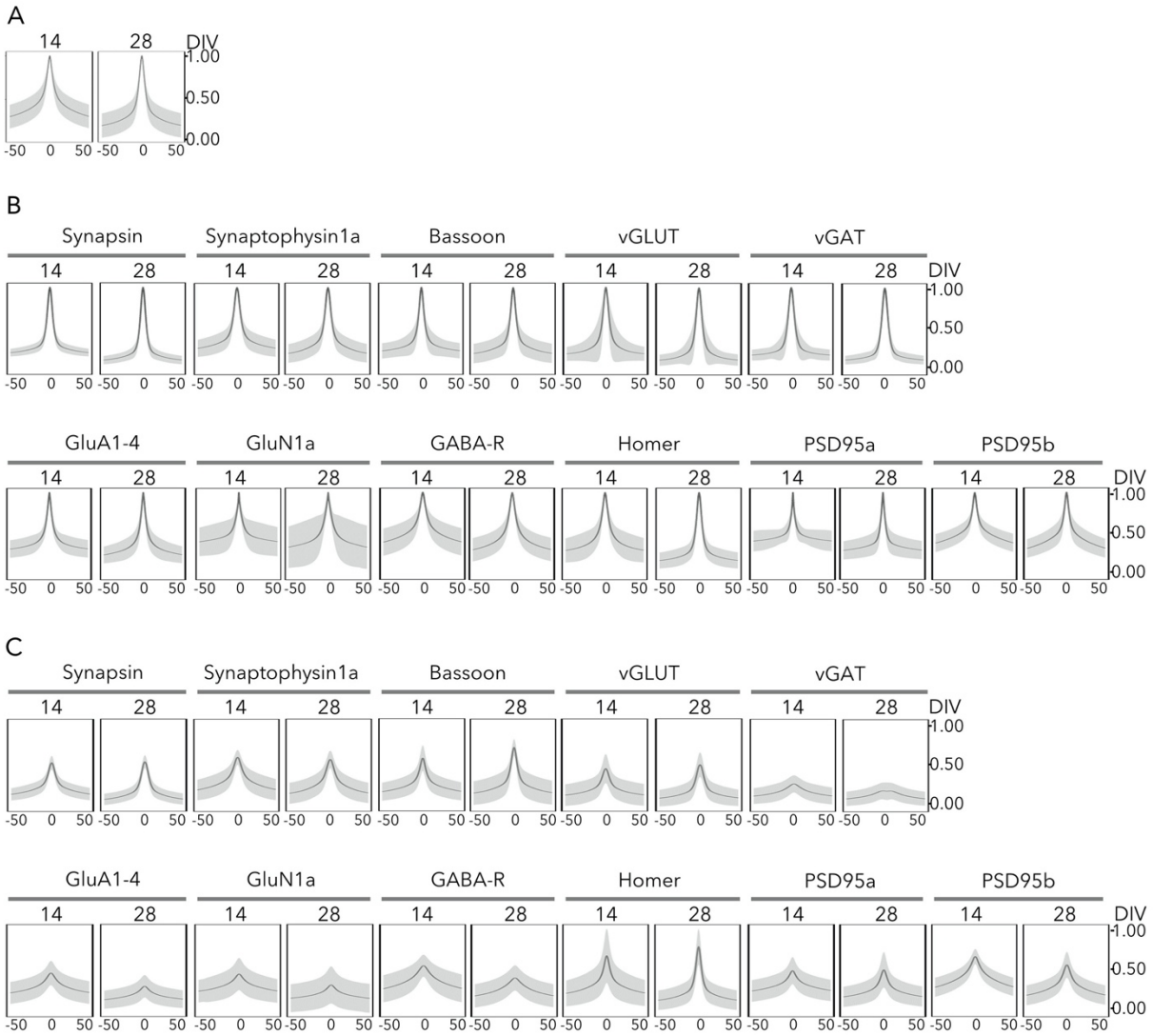

Figure S8. Auto- (A, B) and cross-correlation (C) functions of PSD95-mVenus and synapse markers in hippocampal cultures (n=90 images originating from 6 wells). (Related to Fig. 2)

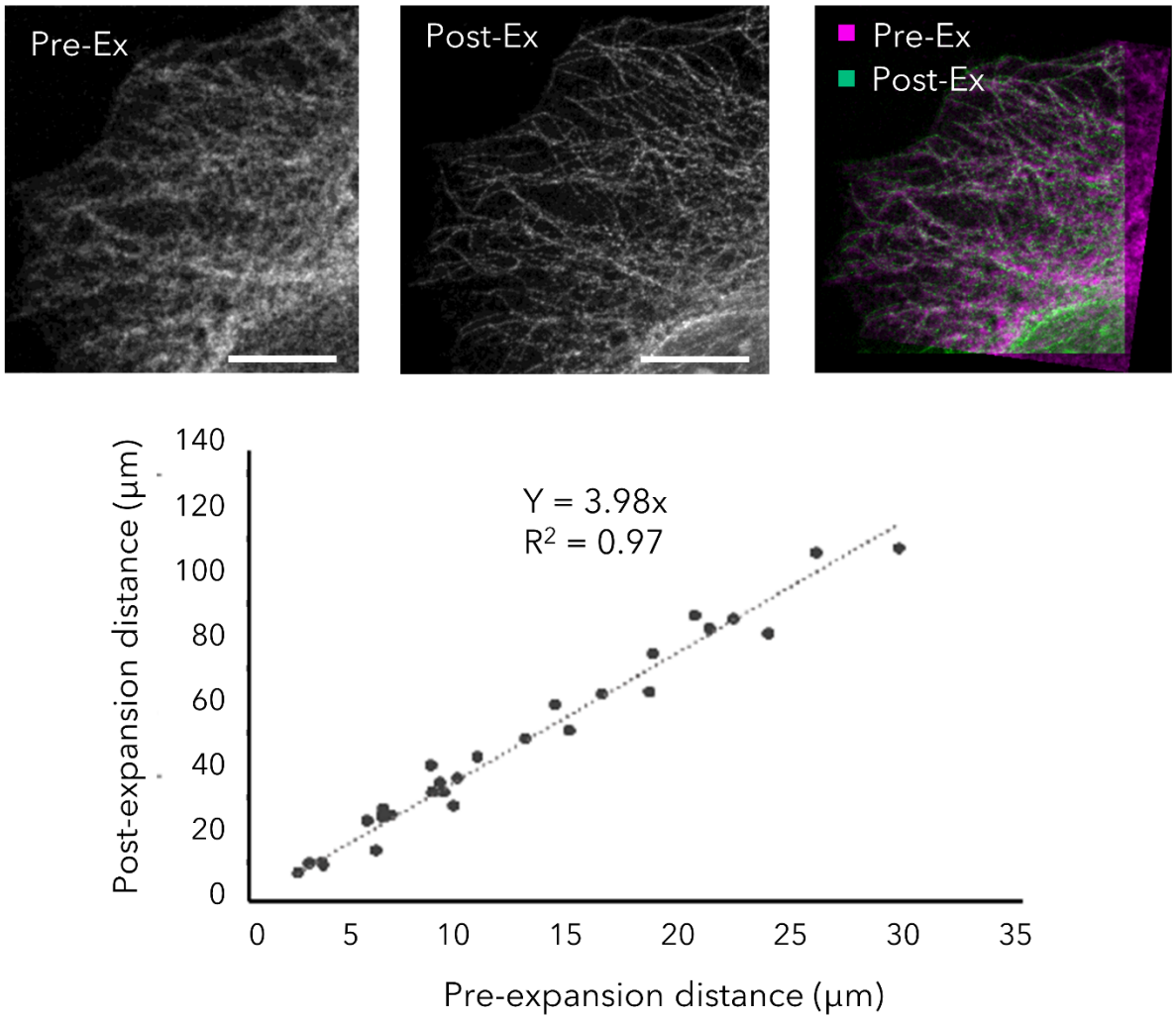

Figure S9. Measurement of the expansion factor in expansion microscopy. (Related to Fig. 3)
HeLa cells were stained for α-tubulin using standard ICC protocols and expansion microscopy was performed using the protocol described by Chozinski et al. (2016). Before digestion of the gel, the samples were imaged a first time. Large sample fields were tile-scanned with a 10x objective to have a topographical overview of the sample. Next, a number of cells were randomly selected within the sample and imaged using a 63x 1.4 NA objective (see 'pre-ex' image as an example; scale bar 25 µm). After the expansion, the same cells were relocated based on the topographical information at low magnification, and cells were reimaged using 63x 1.3 WI objective (see 'post-ex' image for the same example cell; scale bar 100 µm). The green - magenta overlay shows the registration of both images ('Similarity' method in ImageJ: translation + rotation + isotropic scaling, no warping/deformation). To quantify the expansion factor, clearly distinguishable local subcellular hallmark features were manually selected on both the pre- and post-expansion images of the same cells, such as microtubule ends, microtubule crossings or bright signal accumulations, and the distances between those points were measured. The data presented in the scatter plot is from 7 cells originating from two separately expanded samples. The expansion factor for this dataset, as given by the slope of the linear regression line, was 3.98.

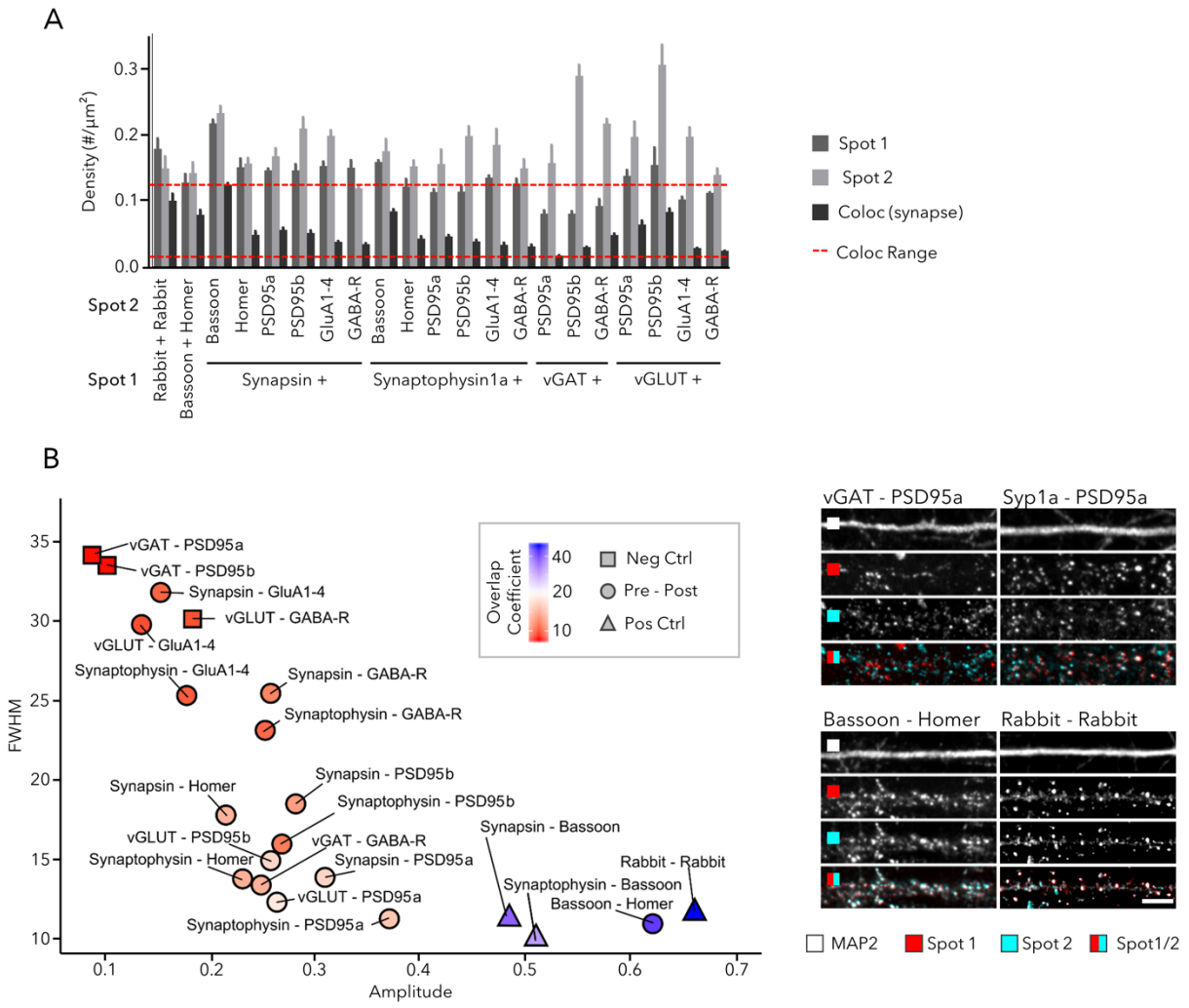

Figure S10. Double labeling of synapse markers in 14 DIV hippocampal cultures. (Related to Fig. 3)
(A) Quantification of spot and synapse density in 14 DIV cortical cultures shows the limited fraction of colocalized signals (Mean + SD, n=6 wells with 15 fields/well); (B) Representative images (scale bar 10 µm) and a scatter plot of CCF parameters reporting on the colocalization of marker pairs in 14 DIV hippocampal neurons (n=90 images originating from 6 wells). The color code indicates the overlap coefficient, defined as the percentage of spots that reside in synapses. Pairs of inhibitory with excitatory synapse markers were considered as negative controls, while two pan-presynaptic markers and primary antibodies raised in the same species were used as positive controls.

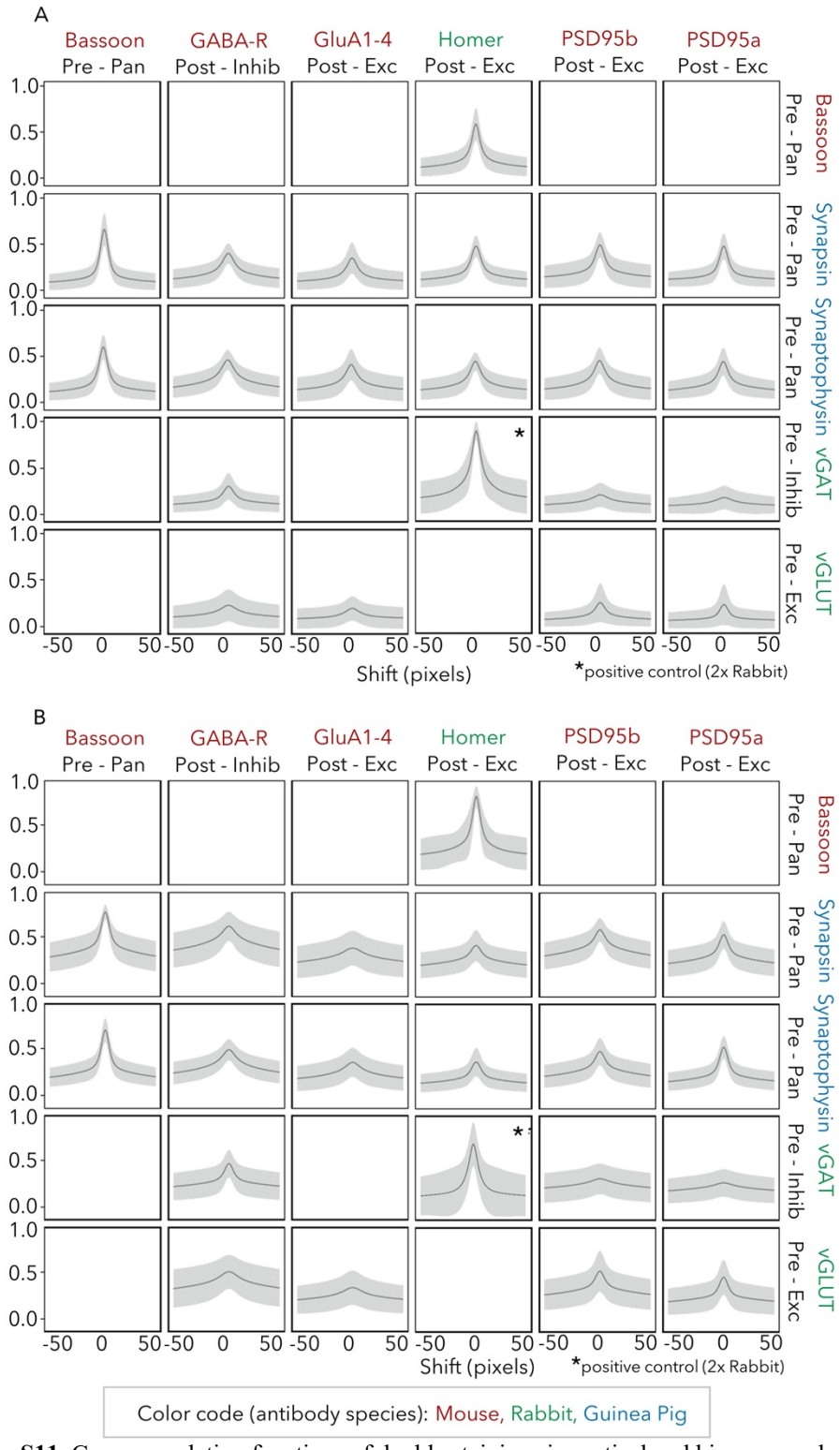

Figure S11. Cross-correlation functions of double stainings in cortical and hippocampal cultures. (Related to Fig. 3) CCFs showing the colocalization (amplitude) and combined length (FWHM) of synapse marker combinations in 14 DIV cortical (A) and hippocampal (B) cultures (n=90 images originating from 6 wells).

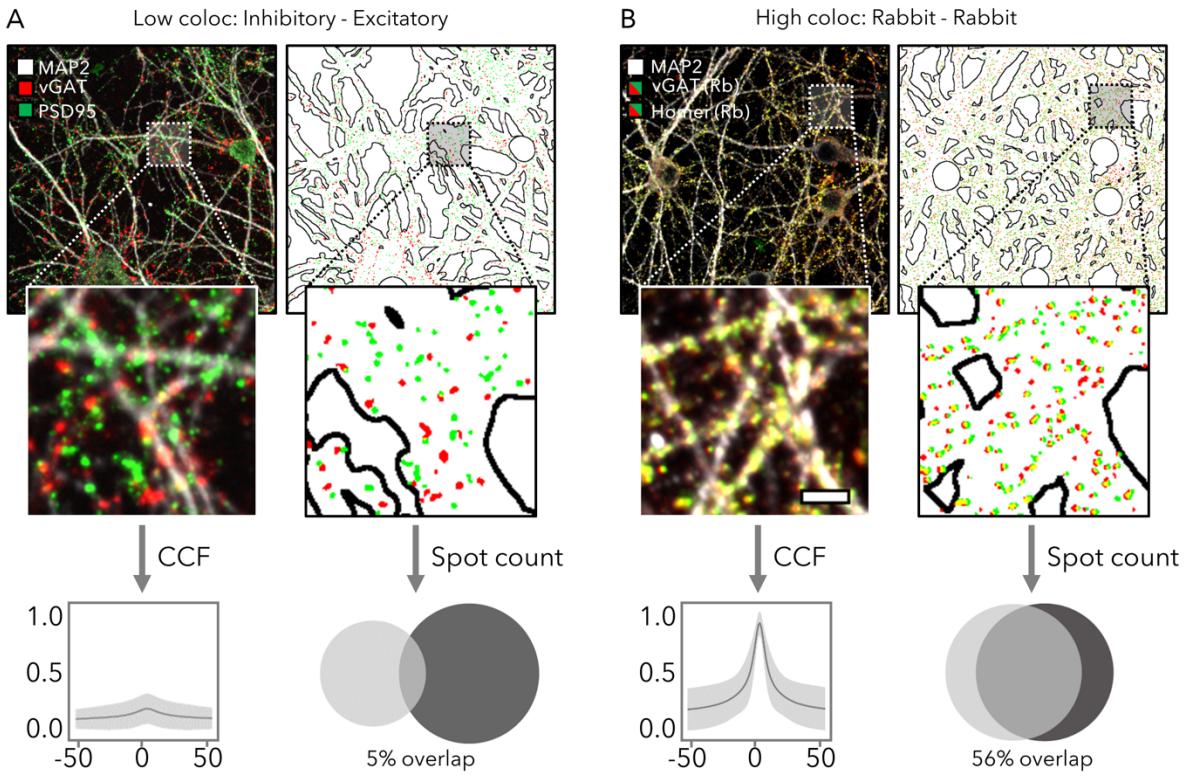

Figure S12. Spot quantification of double stainings with low and high colocalization. (Related to Fig. 3)
(A) The combination of an inhibitory presynaptic (vGAT) with excitatory postsynaptic marker (PSD95a) yields a compact CCF and low OC after segmentation. (B) In contrast, a positive control in which two rabbit primary antibodies are used, yields a CCF that approximates 1 at $\Delta x = 0$ (nearly perfect colocalization), while the OC is still only 56%, displaying the better sensitivity of the segmentation-independent CCF approach. (A-B) n=90 images originating from 6 wells, scale bar 5 µm

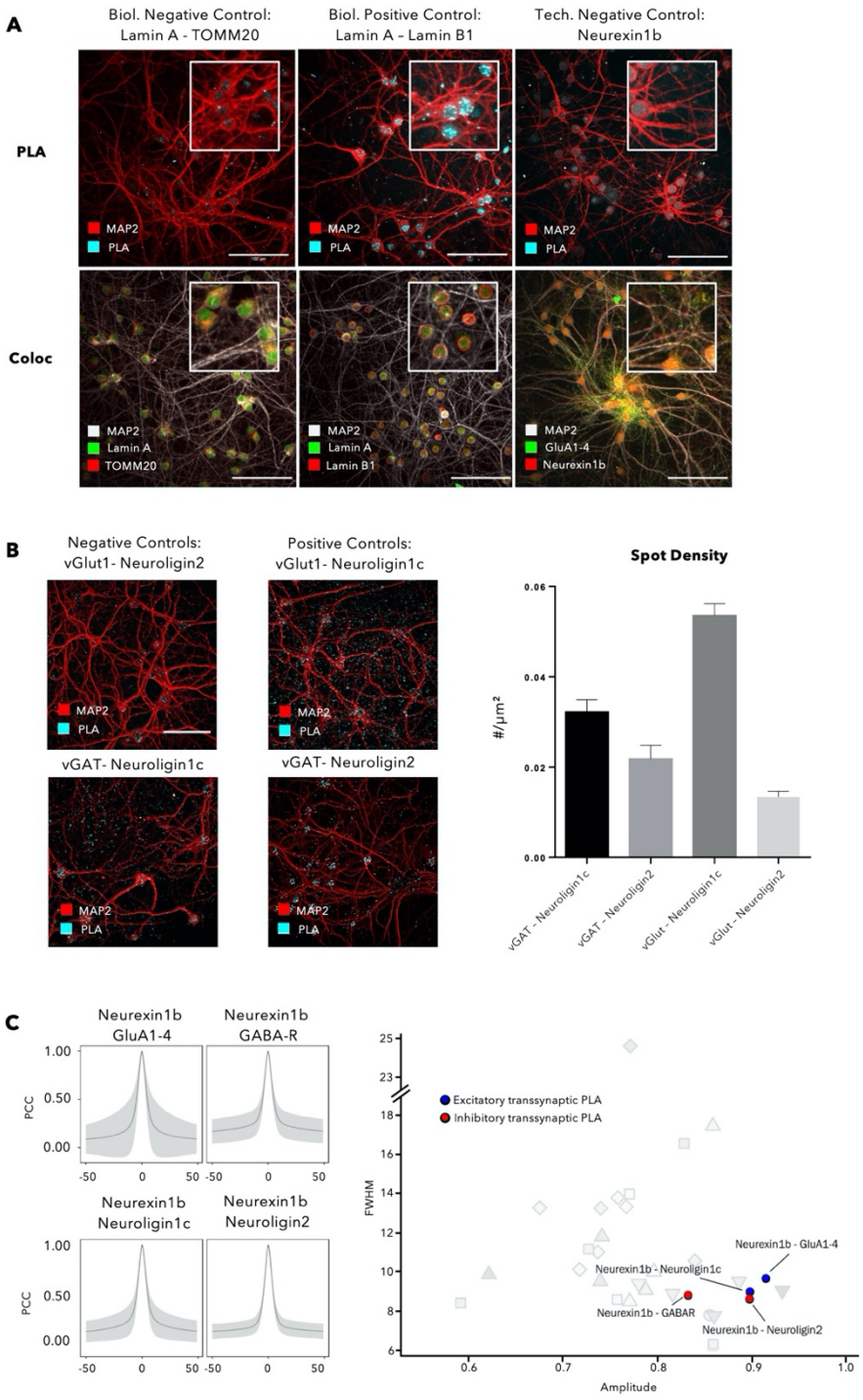

Figure S13. PLA controls and characteristics. (Related to Fig. 4)
(A) Positive and negative technical and biological controls show the specificity of PLA in neurons, when comparing the amount of signal and the location of known interacting nuclear proteins (Lamin A / Lamin B1) with proximal but out-of-PLA-reach markers (Lamin A / TOMM20) as well as the technical control of the omission of a singular primary antibody (scale bar 100 µm); (B) Synaptic PLA with permutations of inhibitory and excitatory markers show that congruent combinations produce increased numbers of PLA spots (mean + SD, n=4 wells with 15 images/well, scale bar 100 µm); (C) ACF plots for PLA signal from specified markers (n=60 images originating from 4 wells); and scatterplot location of synaptic PLA marker combinations as compared with single-staining ACF properties (right, cfr. also **Fig. 1**).

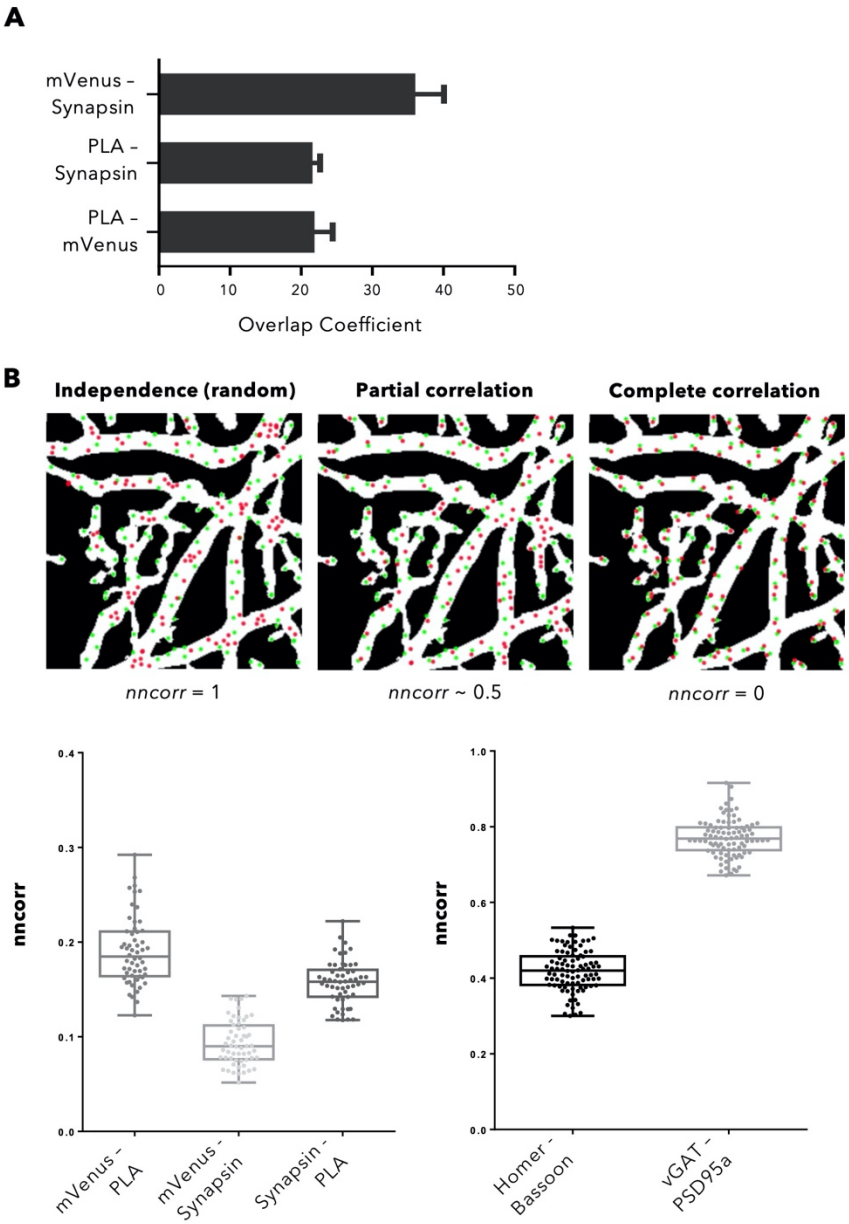

Figure S14. Analyses of PLA triple staining (trans-synaptic PLA-Neurexin1b/Neuroligin1c, mVenus-PSD95 and synapsin) of cortical 28 DIV cultures. (Related to Fig. 4)

(A) Quantification graph of overlap percentage for the specified pairs of spots derived from the segmentation of confocal images. Values are the percentage of each pair against the total number by marker (*e.g.,* PLA – mVenus is the percentage of PLA spots that have an overlapping mVenus signal); (B) Nearest neighbor correlation schematic and quantification. *Nncorr* measures the relationship between two types of spots by calculating the proportion of spots that have a nearest neighbor of the same type, and normalizing by what would be expected from an independent (random) distribution; thus values close to 1 suggest independence between the sets of spots, whereas a value closer to 0 is expected if spots are correlated. PLA triple staining pairs (mVenus-PLA, PLA-synapsin and mVenus-synapsin), present lower *nncorr* values implying that spots are correlated. This was also validated by comparing positive (Homer/Basoon) and negative (VGAT/PSD95a) control IF combinations. Note that in the latter case a different microscopy setup was used, leading to allover higher values (n=4 wells for PLA, n=6 wells for IF 15 field images per well).

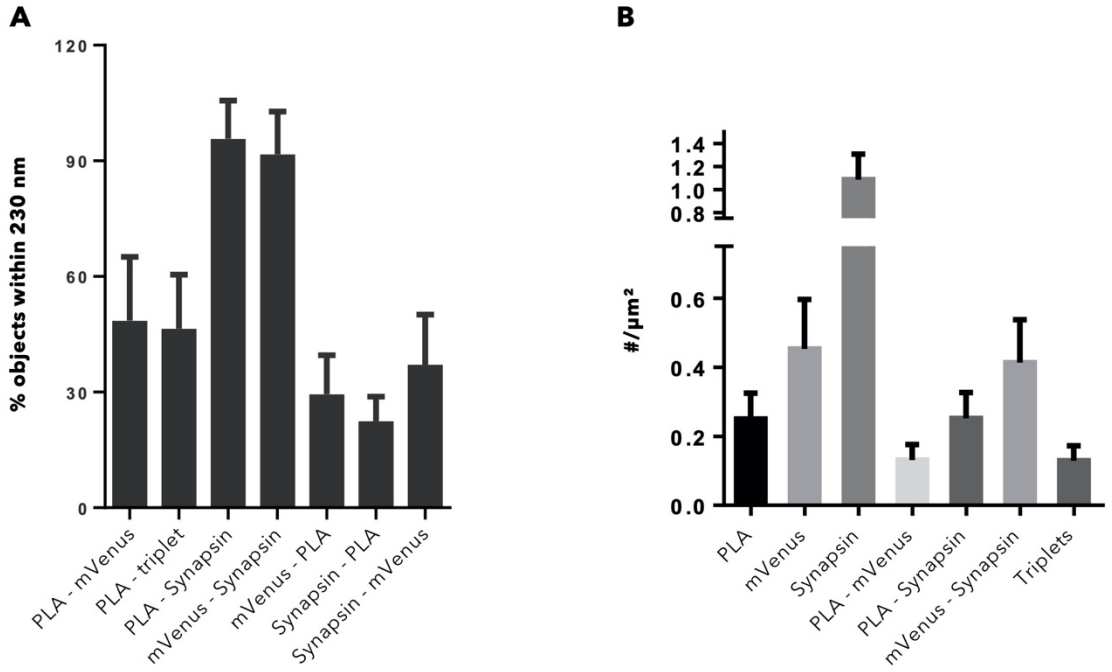

Figure S15. Quantification of spots from SRRF images with triple staining (trans-synaptic PLA, Synapsin and mVenus-PSD95). (Related to Fig. 4)

(A) Quantification of proximity for the specified spots. Spot objects were identified in SRRF images of a single confocal plane of cortical 28 DIV cultures and were then expanded by 10 pixels (~230nm) to identify juxtaposed spots. Values represent the percentage of spots with juxtaposition of another marker spot versus the total number of spots (*e.g.,* PLA – mVenus is the percentage of PLA spots that have an mVenus spot within 230 nm); (B) Spot density for each staining, pairwise combinations and triplets, derived from SRRF images on PLA triple stained cortical 28 DIV cultures (n=4-7 images stacks per PLA combination, 200 frames per image were captured for SRRF)

Table S1. Primary and Secondary antibodies employed in this study (antibodies used in PLA are marked with an asterisk) (Related to transparent methods)

PRIMARY ANTIBODIES

Antigen	Pre/Post	Type	Localization	Epitope	Species/Clonality	Clone	Company	Catalog	Lot	IF conc.	WB conc.
Bassoon	Pre	Pan	Active zone	intracellular	Mouse Monoclonal	L124/59	Neuromab	73-491	463-3DH-50	2 µg/ml	3 µg/ml
Neurexin1a	Pre	Pan	Adhesion	extracellular	Mouse Monoclonal	N170A/1	Neuromab	75-216	447-1JH-73A	20 µg/ml	1 µg/ml
Neurexin1b*	Pre	Pan	Adhesion	Intracellular	Rabbit Polyclonal	NA	Abcam	Ab222806	GR3192323-13	40 µg/ml	1 µg/ml
Synapsin1/2	Pre	Pan	Vesicular	intracellular	Guinea Pig Polyclonal	NA	SySy	106004	106004/1-21	2 µg/ml	0.5 µg/ml
Synaptophysin1a	Pre	Pan	Vesicular	intracellular	Guinea Pig Polyclonal	NA	SySy	101004	101004/2-26	2 µg/ml	0.25 µg/ml
Synaptophysin1b	Pre	Pan	Vesicular	intracellular	Rabbit Polyclonal	NA	Abcam	ab14692	GR200179-2	2 µg/ml	0.65 µg/ml
vGAT	Pre	Inhibitory	Vesicular	intracellular	Rabbit Polyclonal	NA	SySy	131003	131003/1-45	2 µg/ml	0.25 µg/ml
vGlut1	Pre	Excitatory	Vesicular	intracellular	Rabbit Polyclonal	NA	SySy	135303	135303/2-63	2 µg/ml	0.25 µg/ml
AMPA-R (GluA1)	Post	Excitatory	Receptor	extracellular	Mouse Monoclonal	N355/1	Neuromab	75-327	455-5JD-89	2 µg/ml	1 µg/ml
AMPA-R (GluA1-4)*	Post	Excitatory	Receptor	extracellular	Mouse Monoclonal	248B7	SySy	182411	182411/10	2 µg/ml	1 µg/ml
AMPA-R (GluA2)	Post	Excitatory	Receptor	intracellular	Mouse Monoclonal	L21/32	Neuromab	75-002	455-6JD-81C	2 µg/ml	1 µg/ml
GABA-R (β2/3)*	Post	Inhibitory	Receptor	extracellular	Mouse Monoclonal	62-3G1	Neuromab	75-363	455-2JD-15	2 µg/ml	1 µg/ml
Gephyrin	Post	Inhibitory	Scaffold	intracellular	Mouse Monoclonal	L106/93	Neuromab	75-444	455-8JD-47	2 µg/ml	1 µg/ml
Homer1	Post	Excitatory	Scaffold	intracellular	Rabbit Polyclonal	NA	SySy	160003	160003/31	2 µg/ml	1 µg/ml
Neuroligin1a	Post	Excitatory	Adhesion	intracellular	Mouse Monoclonal	N97A/31	Neuromab	75-160	443-2KS-20C	20 µg/ml	1 µg/ml
Neuroligin1b	Post	Excitatory	Adhesion	extracellular	Rabbit Polyclonal	NA	Almone	ANR-035	ANR035AN0125	8 µg/ml	1 µg/ml
Neuroligin1c*	Post	Excitatory	Adhesion	intracellular	Mouse Monoclonal	A-4	Santa Cruz	Sc-365110	B0618	4 µg/ml	1 µg/ml
Neuroligin2*	Post	Inhibitory	Adhesion	intracellular	Mouse Monoclonal	L107/39	Neuromab	75-451	455-8JD-93	20 µg/ml	1 µg/ml
NMDA-R (GluN1a)	Post	Excitatory	Receptor	extracellular	Mouse Monoclonal	N308/48	Neuromab	75-272	455-7JD-90B	2 µg/ml	1 µg/ml
NMDA-R (GluN1b)	Post	Excitatory	Receptor	extracellular	Mouse Monoclonal	M68	SySy	114011	114011/1-24	2 µg/ml	0.25 µg/ml
NMDA-R (GluN2A)	Post	Excitatory	Receptor	extracellular	Mouse Monoclonal	N327/95	Neuromab	75-288	455-7JD-90B	2 µg/ml	1 µg/ml
NMDA-R (GluN2B)	Post	Excitatory	Receptor	extracellular	Mouse Monoclonal	N59/20	Neuromab	73-097	463-1DH-64	2 µg/ml	2 µg/ml
PSD93	Post	Excitatory	Scaffold	intracellular	Mouse Monoclonal	N18/30	Neuromab	75-057	455-3JD-72	2 µg/ml	1 µg/ml
PSD95a	Post	Excitatory	Scaffold	intracellular	Mouse Monoclonal	7E3-1B8	ThermoFisher	MA1-046	SA242215	2 µg/ml	0.5 µg/ml
PSD95b	Post	Excitatory	Scaffold	intracellular	Mouse Monoclonal	K28/43	Neuromab	75-028	455-7JD-22F	2 µg/ml	1 µg/ml
SAP102	Post	Excitatory	Scaffold	intracellular	Mouse Monoclonal	N19/2	Neuromab	75-058	449-1AK-85B	2 µg/ml	1 µg/ml
Shank 1/2/3	Post	Excitatory	Scaffold	intracellular	Mouse Monoclonal	N23B/49	Neuromab	75-089	443-1KS-78B	2 µg/ml	1 µg/ml
MAP2	NA	NA	Dendrite	intracellular	Chicken Polyclonal	NA	SySy	188006	188006/1-3	2 µg/ml	NA
GAPDH	NA	NA	Cytoplasm	intracellular	Mouse Monoclonal	GT239	GeneTex	GTX627408	41323	NA	1 µg/ml
GFP/mVenus	NA	NA	NA	intracellular	Alpaca Monoclonal	+Atto594	Chromogen	Gba594	81212001AT3	1 µg/ml	NA

SECONDARY ANTIBODIES

Type	Conjugate	Company	Catalog	Lot	Concentration
Donkey-anti-Guinea Pig	HRP	Jackson Immunoresearch	706-035-148	128221	0.1 µg/ml
Donkey-anti-Mouse	HRP	Jackson Immunoresearch	715-035-151	125909	0.5 µg/ml
Donkey-anti-Rabbit	HRP	Jackson Immunoresearch	711-035-152	104907	0.2 µg/ml
Donkey-anti-Chicken	AlexaFluor647	Jackson Immunoresearch	703-605-155	134612	1 µg/ml
Goat-anti-Mouse	AlexaFluorPlus488	ThermoFisher	A32723	SG251135	2 µg/ml
Goat-anti-Rabbit (Fab)	FITC	Jackson Immunoresearch	111-097-003	104632	0.5 µg/ml
Donkey-anti-Guinea Pig	Cy3	Jackson Immunoresearch	706-165-148	127715	1 µg/ml
Donkey-anti-Mouse	Cy3	Jackson Immunoresearch	715-165-151	125797	1 µg/ml
Goat-anti-Rabbit (Fab)	Cy3	Jackson Immunoresearch	111-167-003	78942	0.5 µg/ml

Transparent Methods

Primary neuronal cell culture

The preparation of primary neuronal cultures was carried out in accordance with the recommendations of the ethical committee for animal experimentation of the University of Antwerp (approved ethical file 2015-54). Hippocampi and cortex were dissected from wild type C57Bl6 and PSD95-CreNABLED (Fortin et al., 2014) (purchased from the Jackson Laboratories, ref 029242) E18 mouse embryos in HEPES (7 mM)-buffered Hanks Balanced Salt Solution (HBSS-HEPES), followed by trypsin digestion (0.05%; 10 min; 37°C) and mechanical dissociation. After centrifugation (5 min at 200g), the cell pellet was resuspended in Minimal Essential Medium supplemented with 10% heat-inactivated normal horse serum and 30 mM glucose. Cells were plated in Poly-D-Lysin-coated 96-well plates (Greiner µClear) at 30,000 cells/cm² (for immunocytochemistry), or in 6-well plates at 60,000 cells/cm² (for western blot) and kept in a humidified CO_2 incubator (37°C; 5% CO_2). After 4 hours, the medium was replaced with 150 µl B27-supplemented Neurobasal medium (NB-B27), containing Sodium Pyruvate (1 mM), Glutamax (2 mM), glucose (30 mM) and Penicillin-Streptomycin (0.5%). To suppress proliferation of non-neuronal cells, 0.5 µM arabinosylcytosine was added in 25 µl NB-B27 at the third and tenth day *in vitro* (DIV). AAV6-mediated transduction of hTau-P301L was done at 3 DIV. Cell culture supplies were purchased from ThermoFisher (Waltham, MA, USA).

Western blotting

14 DIV cortical and hippocampal cultures were lysed using ice-cold RIPA buffer supplemented with phosphatase and protease inhibitor (HALT cocktail, ThermoFisher 78445) and 5 mM EDTA. The lysate was centrifuged (10,000g, 20 min, 4 °C) and the protein concentration of the supernatant was determined using a BCA assay (ThermoFisher 23225). Samples were denatured (70% sample, 25% LDS, 5% DTT) for 10 min at 70 °C before being loaded on a 4-12% Bis-tris gel (ThermoFisher NP0322BOX) at 10 µg/lane. A stained ruler was included in the third and eight well (ThermoFisher 26616). The gel tank was filled with NuPage MOPS SDS running buffer and NuPage anti-oxidant, and was cooled during electrophoresis (200V, ± 1h). Proteins were transferred to a PVDF membrane using NuPage transfer buffer (30V, 1h). To check the transfer, blots were reversibly stained with a 0.1% Ponceau S solution in 5% acetic acid. Blots were subsequently blocked with 5% ECL blocking solution in Tris-buffered Saline with 0.1% Tween (TBS-T). Using the rulers as landmakrs, blots were cut into five pieces so that two lanes (hippocampal and cortical) with or without the ruler could be stained in one reaction. Primary antibody was applied overnight at 4 °C on a roller, followed by a TBS-T wash (3 x 5 min). Horse Radish Peroxidase-coupled secondary antibodies were incubated for 2h at room temperature (RT), followed by a final TBS-T wash. All antibodies were diluted in blocking buffer and are listed in **Table S1**. After reconstructing the cut blots into their original positions, bioluminescent detection was performed using Immobilon Western HRP substrate (Merck Millipore WBKLS0500, 30 sec) and a Chemidoc Touch imager (Bio-Rad, Temse, Belgium). After completion, the blots were restained for GAPDH as loading control. The global contrast of the individual (cut) blots was adjusted with Fiji image analysis freeware (Schindelin et al., 2012). The positions of the molecular weight markers were written on the blots after overlaying the bioluminescent image with its marker (visible spectrum).

Immunofluorescence staining (IF)

Paraformaldehyde-fixed cultures (2%, 20 min, RT) were permeabilized with 1% Triton X-100 in blocking buffer (0.1% bovine serum albumin and 10% normal horse serum in PBS) for 10 min, followed by an overnight incubation with the primary antibodies (**Table S1**) at 4 °C in blocking buffer. After washing with PBS, secondary antibodies (**Table S1**) were added for 2h. Finally, 4′,6-diamidino-2-phenylindole (DAPI) was applied to the cultures for 10 min at a concentration of 2.5 µg/ml, followed by a PBS wash. Primary antibodies targeting extracellular epitopes were incubated prior to permeabilization to reduce non-specific intracellular background staining. This was followed by a PBS wash and permeabilization to continue with antibodies targeting intracellular epitopes. All presynaptic markers were designated to the 561 nm excitation channel, while postsynaptic markers were labeled for the 488 nm channel. Secondary antibodies were kept identical where possible, depending on the species of the primary antibody.

Expansion microscopy

The protocol for expansion of the samples was adapted from (Chozinski et al., 2016). In brief, immunostained samples were crosslinked for 10 min in 0.25% glutaraldehyde in PBS. Gelation was done in a mixture of 2M NaCl, 2.5% (w/w) acrylamide, 0.15% (w/w) N,N'-methylenebisacrylamide, 8.625% (w/w) sodium acrylate in PBS with polymerization initiated with TEMED and APS. Polymerized gels were incubated for 30 min at 37°C in a digestion buffer containing 8 U/ml proteinase K. Cover glasses were removed from the digested gels, which were placed in high volumes (> 30 mL) of distilled water that were exchanged at least five times until full expansion of the gels. Finally, the gels were

trimmed, nuclei counterstained with Hoechst 33342 (1/5000 in water for 30 min at room temperature), positioned in 50 mm diameter glass bottom dishes (WillCo Wells GWSt-5040) and immobilized using 2% agarose. The lateral expansion factor of samples processed identically to those shown throughout the manuscript was calculated to be 3.98, based on distance measurements between of the same cellular hallmark structures imaged pre- and post-expansion (**Fig. S9**). This is in line with the expansion factor described in the original protocols (Chozinski et al, 2016; Chen et al., 2015). In an approximation, this expansion factor was applied to all other experiments.

Dendritic spine labeling
To label spines in a sparsely distributed subset of neurons, 14 DIV cultures were incubated with the lipophilic dye CM-DiI (ThermoFisher C7000, 5 µg/ml, 20 min), followed by a PBS wash. The next day, after the dye had spread throughout the plasma membrane, the cultures were gently permeabilized using a glycerol gradient (50% glycerol for 20 min, 80% for 20 min and 100% for 50 min) followed by an extensive PBS wash. This permeabilization protocol preserved DiI fluorescence while allowing antibody penetration. A similar, but longer protocol was used for IF, in which the primary antibody was applied overnight at RT and the secondary for 4 hours.

Synaptic Proximity Ligation Assay (synaptic PLA)
Primary cultures fixed and permeabilized as described for IF were used to perform PLA using a commercial kit (Duolink® PLA starter kit, Sigma-Aldrich, Overijse, Belgium) according to the manufacturer's instructions. Briefly, cells were incubated with a commercial blocking buffer, and then incubated overnight at 4°C, with primary antibodies diluted in the commercial solution at concentrations described in **Table S1**. After PLA probe incubation, ligation and amplification steps, samples were immunostained for MAP2 and Synapsin for triple staining experiments, counterstained with Duolink® Nuclear Stain and mounted with anti-fade buffer (Sigma-Aldrich). Images were taken no more than two days after the PLA procedure to ascertain signal preservation.

Microscopy
Cultures were imaged with a spinning disk confocal high-content imager (Opera Phenix, PerkinElmer) equipped with a robotic arm for plate loading. A 40X water immersion objective (numerical aperture (NA) 1.1) was used. At 488 nm excitation, the optical resolution of the system is 0.271 µm (and corresponding pixel size 0.149 µm), which is considerably larger than the distance of the synaptic cleft (15–25 nm), yet sufficiently small to allow signals of corresponding pre- and postsynaptic markers to partially overlap. Per well, 15 fields were acquired in four channels (405nm, 488nm, 561nm and 640nm excitation) at four axial positions separated by 1 µm spacing. Different fluorescence channels were separated using standard excitation/emission filters and dichroic mirrors. Owing to the large dynamic range of the Opera Phenix system, acquisition settings could be kept identical for all experiments. For assessing localization of postsynaptic markers in dendritic spines and triple stainings (trans-synaptic PLA/mVenus/Synapsin), a spinning disk confocal research microscope (UltraVIEW VoX, PerkinElmer) was used, equipped with a 60X water objective (NA 1.2) resulting in an optical resolution of ~200 nm and corresponding pixel size of 120 nm. Finally, for super-resolution radial fluctuations (SRRF) microscopy (Culley et al., 2018), the same setup was used to acquire stacks of 200 images of the same confocal plane, using the Perfect Focus System to prevent focus drift.

Image analysis
To assess the degree of colocalization between two synaptic markers, we adopted the *van Steensel* approach (van Steensel et al., 1996), which we implemented via a home-written script for Fiji image processing freeware. This method calculates the Pearson's correlation coefficient (PCC) between two images as a function of a lateral shift (Δx), resulting in a correlation function (CF). When the image is compared to its (shifted) duplicate, the result is an auto-correlation function (ACF). In case of complete colocalization, the correlation function (CF) has a maximum (PCC = 1) at $\Delta x = 0$ (no shift); in case of exclusion, it reaches a minimum at this position. The shape of the CF not only informs on the presence or absence of colocalization, when colocalization is present, it also provides information on the size of the overlapping spots (the width of the CF measured as full width at half maximum (FWHM)) and the dynamic range – and thus quality – of the staining (measured as the amplitude of the CF). Exactly because of this latter property, the approach was also used to assess the specificity of single synapse marker staining, the assumption being that the ACF of an image decreases with Δx much stronger for a specific staining than it does for less specific ones. The maximal pixel shift used for both analyses was 50 pixels in both directions, which is well beyond the typical spot diameter of ~ 10 pixels. The variation across images, or the spread, was expressed by a band of 1 standard deviation above and below the average cross-correlation function (CCF) and measured at $dx = 50$ px for plotting. The auto- or cross-correlation function (ACF/CCF) reports on labeling performance without differentiating between specificity,

sensitivity or local antigen abundance, as its amplitude will increase when background signal arising from non-specific binding is low, more target epitopes are labeled and when epitopes are highly enriched in synapses. Given that no preprocessing or segmentation is required, the CF method is not sensitive to user bias, yet it is influenced by the magnification and image resolution (**Fig. S3A-C**) which is why all acquisitions were done with one and the same objective lens (40X NA 1.1). Given the high density and heterogeneous distribution of the synaptic spots, the orientation of the sliding window does not significantly influence the readout (**Fig. S3D**).

Spot and synapse density quantification was carried out in Acapella® software (PerkinElmer). Nuclei (DAPI) and neurites (MAP2) were segmented based on a user-defined fixed threshold. Non-neuronal nuclei were removed based on their larger size, lower circularity and limited overlap with the neurite mask. Next, both the neurite and neuronal nuclei mask were dilated and subtracted from each other to obtain a search region for synapse marker spots. Spots were enhanced using a Difference of Gaussian filter with a ratio of 1.6. To set thresholds in an unbiased manner, a Fiji script was written that allowed user-friendly interaction with the images while being blinded for the synapse marker at hand. Spot counts were normalized to the neurite area to obtain the spot density. For double stainings and PSD-mVenus experiments, the density of colocalizing spots in two fluorescence channels was calculated as those spots for which at least one-pixel overlaps. We previously determined that measurements were not biased by chromatic aberration using fluorescent beads (the lateral and axial shifts between channels were below one pixel and manually introduced one-pixel shifts did not affect the colocalization measurement significantly) (Verschuuren et al., 2019). For colocalization of antibodies with PSD95-mVenus, the percentage of PSD95-mVenus spots with an overlapping synapse marker spot was measured. For double immunostainings, the percentage of all spots that reside in synapses was calculated as the density of colocalizing spots divided by the density of all (colocalizing and non-colocalizing) spots multiplied by 100.

For double labeling with dendritic spines, the puncta within a CM-DiI-positive stretch were counted manually on anonymized images and assigned to either the dendritic shaft or spine. The percentage of spots residing in dendritic spines, and the percentage of spines containing spots were calculated. To quantify trans-synaptic PLA spot density on samples counterstained with MAP2, the same Acapella® script was used as described above. For nearest neighbor analyses, center coordinates were extracted for all spots (using a similar CellProfiler pipeline as described for Acapella®), and the pairwise distance distribution between spot types (PLA, mVenus, Synapsin) was analyzed in R using the package *spatstat* by applying the nearest neighbor correlation (*nncorr*) method after correcting for the search region (neurite mask) (Baddeley and Turner, 2005). For SRRF, the NanoJ plugin for Fiji was used (Culley et al., 2018). Briefly, after drift correction with NanoCore, a temporal radial auto-correlation of order 2 was applied, with gradient smoothing, intensity weighting and gradient weighting (point spread function FWHM = 3.17) for spot channels, and the previous settings with renormalization for the MAP2/DAPI channel. To account for the increase in resolution, subsequent spot overlap was determined between different channels of the SRRF images after expanding detected objects with 10 pixels (~240 nm). The center locations of the detected spots were used to calculate the average nearest neighbor distance between marker combinations with *the nndist* and *marktable functions* of the *spatstat* R package.

Data visualization and statistics

For displaying purposes, the contrast of each fluorescence channel was optimized and this was done for the entire image. Graphs were constructed in Graphpad Prism and statistics performed in SAS JMP. The number of replicates is indicated in the figure legends. For segmentation-independent Steensel analyses, 90 images originating from six wells were considered per condition (marker or marker combination and cell type), and for spot segmentation the same number of images were considered but averaged per well (n=6 wells with 15 images/well). For dendritic spine analysis, at least 200 spines were counted per condition. For trans-synaptic PLA experiments 4 or 8 wells with 15 fields per well were averaged per condition. For SRRF of trans-synaptic PLA staining, between of four and seven images were used per combination. For statistical comparison of spot densities, a one-way ANOVA was performed followed by post-hoc testing for predefined comparisons (antibodies that had the same target; seven comparisons) with Sidak's correction. For triple stainings, a two-way ANOVA was performed with marker and PLA type as fixed factors, post-hoc tests for comparisons within conditions are specified in the results. For hTau-P301L overexpression a two-way ANOVA was performed with staining type and MOI as fixed factors, followed by post-hoc testing for predefined comparisons (to MOI 0 within each staining type) with Sidak's correction.

Supplemental References

Chen, F., Tillberg, P.W., and Boyden, E.S. (2015). Optical imaging. Expansion microscopy. Science *347*, 543-548.

Chozinski, T.J., Halpern, A.R., Okawa, H., Kim, H.J., Tremel, G.J., Wong, R.O., and Vaughan, J.C. (2016). Expansion microscopy with conventional antibodies and fluorescent proteins. Nat. methods *13*, 485-488.

Culley, S., Tosheva, K.L., Matos Pereira, P., and Henriques, R. (2018). SRRF: Universal live-cell super-resolution microscopy. Int. J. Biochem. Cell B *101*, 74-79.

Schindelin, J., Arganda-Carreras, I., Frise, E., Kaynig, V., Longair, M., Pietzsch, T., Preibisch, S., Rueden, C., Saalfeld, S., and Schmid, B., et al. (2012). Fiji: an open-source platform for biological-image analysis. Nat Methods *9*, 676-682.